

OH(1720 MHz) Masers As Signposts of Molecular Shocks

Dale A. Frail¹ and George F. Mitchell²

ABSTRACT

We present observations of molecular gas made with the 15-m James Clark Maxwell Telescope toward the sites of OH(1720 MHz) masers in three supernova remnants: W 28, W 44 and 3C 391. Maps made in the $^{12}\text{CO } J = 3 - 2$ line reveal that the OH masers are preferentially located along the edges of thin filaments or clumps of molecular gas. There is a strong correlation between the morphology of the molecular gas and the relativistic gas traced by synchrotron emission at centimeter wavelengths. Broad CO line widths ($\Delta V=30\text{-}50 \text{ km s}^{-1}$) are seen along these gaseous ridges, while narrow lines are seen off the ridges. The ratio of H_2CO line strengths is used to determine temperatures in the broad-line gas of 80 K, and the $^{13}\text{CO } J = 3 - 2$ column density suggests densities of $10^4\text{-}10^5 \text{ cm}^{-3}$. These observations support the hypothesis that the OH(1720 MHz) masers originate in post-shock gas, heated by the passage of a supernova remnant shock through dense molecular gas. From the observational constraints on the density, velocity and magnetic field we examine the physical properties of the shock and discuss the shock-production of OH. These OH(1720 MHz) masers are useful “signposts”, which point to the most promising locations to study supernova remnant/molecular cloud interactions.

Subject headings: ISM: supernova remnants, molecules – ISM: individual (W28, W44, 3C391) – masers

¹National Radio Astronomy Observatory, Socorro, NM, 87801, USA

²Department of Astronomy and Physics, Saint Mary’s University, Halifax, NS B3H 3C3, CANADA

1. Introduction

It has recently been argued that a satellite line ($\nu_o = 1720.53$ MHz) from the ground state of the hydroxyl radical (OH) is a powerful tracer for studying the interaction of supernova remnant shocks with molecular clouds (Frail, Goss & Slysh 1993). Bright OH(1720 MHz) maser emission has been detected towards 17 supernova remnants (10% of the observed sample) in our Galaxy (Green et al. 1997). On the basis of this positional and velocity coincidence the case can be made that the OH(1720 MHz) masers in supernova remnants are a separate class of OH masers in our Galaxy, distinct from the OH masers in star-forming regions and those in the circumstellar shells of late-type stars.

Both observationally and theoretically there is support for the hypothesis that the masers are collisionally excited by H₂ heated by the passage of a shock. Early theoretical work by Elitzur (1976) showed that collisions of OH with H₂ can create a strong inversion of the 1720 MHz line for a range of kinetic temperatures ($25 \text{ K} \leq T_k \leq 200 \text{ K}$) and molecular gas densities ($10^3 \text{ cm}^{-3} \leq n_{\text{H}_2} \leq 10^5 \text{ cm}^{-3}$) which are typical of the conditions expected in cooling post-shock clouds. Pavlakis & Kylafis (1996a,b) have included the effects of far infrared line overlap (due to thermal and turbulent motions) and used newly computed collisional cross sections between OH and H₂ to confirm Elitzur’s basic result for a limited range of $T_k=100$ to 200 K.

The observational evidence that the OH(1720 MHz) masers originate in the post-shock gas is less compelling, relying mostly on indirect and morphological indicators (see Green et al. 1997). What is missing for the most part are clear kinematic and chemical signatures of a molecular shock in the vicinity of the OH(1720 MHz) masers. This situation has begun to change. For the well-studied IC 433 there is a clear kinematic shock signature at the location of the masers (van Dishoeck, Jansen & Phillips 1993), and for W 44 and 3C 391 Reach and Rho (1996) detected local emission maxima for the important cooling line of [OI] at the location of several OH(1720 MHz) masers. In this paper we detail a molecular line study undertaken toward the sites of several OH(1720 MHz) masers with the aim of testing whether they originate in post-shock molecular gas.

2. Observations

The observations were made over 4 nights from 1997 July 20 to 23 using the 15-m James Clark Maxwell Telescope (JCMT). We made ¹²CO $J = 3 - 2$ raster maps around four OH(1720 MHz) maser sites toward three supernova remnants: W 28, W 44 and 3C 391. The mapped regions in W 28 and W 44 are designated as W 28F, W 44E and W 44F in Claussen et al. (1997), while for 3C 391 we mapped the region around the southernmost maser (Frail et al. 1996). Details are given in Table 1.

At several of the intensity peaks found in the CO maps, we obtained spectra of a number of other molecules. These observations and results will be discussed in detail in a subsequent paper.

Here we make use only of the $^{13}\text{CO } J = 3 - 2$ (330.588 GHz), $\text{H}_2\text{CO } 3_{03}-2_{02}$ (218.222 GHz), $\text{H}_2\text{CO } 3_{22}-2_{21}$ (218.475 GHz), and $\text{H}_2\text{CO } 5_{05}-4_{04}$ (362.736 GHz) transitions. The $3 - 2$ transitions of H_2CO required the facility A-band receiver, with a beamwidth of $20''$ and a main beam efficiency of 0.79.

3. Results

In Plates 1 and 2 we show maps of integrated CO $J = 3 - 2$ emission together with representative spectra at several locations. The maser positions are also superimposed on these maps. The velocity data cubes of these pointings show a rich variety of complex structure, but we will defer a detailed discussion of these for another paper. Here we present evidence which indicates the existence of molecular shocks in the vicinity of the OH(1720 MHz) masers.

It is apparent in Plates 1 and 2 that the masers are not located at random with respect to the molecular gas but rather are found near the peaks in the integrated CO $J = 3 - 2$ maps. In one striking example the line of nine masers in W 44E nicely delineates the forward edge of the molecular gas, closest to the shock. Claussen et al. (1997) have suggested that this line of masers traces the shock front from W 44 which is moving eastward into the ambient molecular gas. The morphology of this gas is also noteworthy as it is concentrated in well-defined filaments or clumps. These features are largely unresolved by our $13''$ beam in one dimension but are 1 pc to 2 pc long in the other. In W 44F, for example, a thin filament of gas can be traced from the northwest to the southeast across the entire $70'' \times 75''$ map. It is likely that the true extent of these features is not revealed by these figures since we have mapped only a small fraction ($< 1\%$) of each supernova remnant. With few exceptions, the masers are preferentially located nearer to the edge of the shock (as traced by the non-thermal emission) than the peak of the CO itself. This suggests that some special conditions are required in order to produce a strong inversion of the OH molecule.

Another interesting correlation can be discerned between the integrated CO $J = 3 - 2$ maps and the radio continuum images found in Claussen et al. (1997) and Wilner et al. (1998). Near W 44F the radio continuum contours have the same orientation as the molecular filament and a local maxima in the non-thermal radio continuum of W 44F coincides with the peak in the CO $J = 3 - 2$ map. Likewise, for 3C 391 the radio continuum and the molecular clump have the same curvature while for W 28F a prominent "kink" can be seen in in both the molecular gas and the radio continuum. Local increases in the synchrotron emissivity do not require new particle acceleration, but rather can originate from the compression of the magnetic field and existing relativistic electrons in a radiative shock (Blandford & Cowie 1982). While good correlations have been noted between the optical line and radio continuum emission of several supernova remnants (e.g. Cygnus Loop: Straka et al. 1986), this is the first clear signature to our knowledge of a synchrotron/molecular correlation.

Although the morphology of the molecular gas is suggestive of a shock interaction, it is the velocity extent of the lines that are the most telling. Spectra taken near the peaks and along

the ridges of the integrated CO $J = 3 - 2$ emission (see Figs. 1 and 2) consistently show broad, asymmetric lines whose widths ($\Delta V = 30\text{--}50 \text{ km s}^{-1}$), reminiscent of those seen toward IC 433 (van Dishoeck et al. 1993). Away from the bright peaks the line widths narrow considerably ($\Delta V \leq 10 \text{ km s}^{-1}$) (e.g. Fig. 1). Moreover, whenever it is possible to identify this less disturbed gas, its LSR velocity agrees with that of any nearby masers to within a few km s^{-1} . Examples include 3C 391 where a narrow line component in CO emission at $+105.5 \text{ km s}^{-1}$ is found widely distributed in the region which includes the OH(1720 MHz) maser at 104.9 km s^{-1} (see also Reach and Rho 1998). In W 44E and W 44F there are what appear to be narrow, self-absorption features at $+43$ and $+46 \text{ km s}^{-1}$, respectively. Although they too are close to the mean LSR velocity of the masers in each direction, some caution is warranted since false absorption may be introduced by our sky switching calibration cycle. The correspondence between the maser velocities and colder, presumably unshocked ambient medium is expected since it has been argued elsewhere (Claussen et al. 1997) that these masers originate in shocks which are viewed largely transverse to the line of sight.

For the bright CO peak at $(15'', -40'')$ in the W 28F map (Plate 1), we have also observed the three H_2CO transitions $3_{03}\text{--}2_{02}$, $3_{22}\text{--}2_{21}$, and $5_{05}\text{--}4_{04}$ to determine both gas kinetic temperature and gas density. The importance of H_2CO in measuring T_k and n is described in detail in Mangum & Wootten (1993). The intensity ratio $3_{03}\text{--}3_{02}/3_{22}\text{--}3_{21}$ provides the gas kinetic temperature, either from LVG analysis (e.g. Mangum & Wootten 1993; van Dishoeck et al. 1993) or using LTE expressions (Mangum & Wootten 1993). The observed intensity ratio in W 28F is 3.25, implying $T_k = 80 \pm 10 \text{ K}$. This high value of T_k is further evidence of a shock. When T_k is known, the ratio $3_{03}\text{--}2_{02}/5_{05}\text{--}4_{04}$ provides the gas density. With $T_k = 80 \text{ K}$, we interpolated between LVG models of Mangum & Wootten (1993), using the observed 3-2/5-4 ratio of 1.5 to find $n_{\text{H}_2} = 2 \times 10^6 \text{ cm}^{-3}$.

We have $^{13}\text{CO } J = 3 - 2$ spectra at ^{12}CO intensity peaks in W 28F, W 44E, and 3C 391. Because the critical density for excitation of CO is low, level populations probably follow a Boltzmann distribution. Assuming LTE, it is straightforward to obtain from the line ratio $^{12}\text{CO}/^{13}\text{CO}$ the optical depth, the excitation temperature, and the CO column density (e.g. Mitchell et al. 1992). The observed beam-averaged column densities yield a gas number density if we know the line-of-sight extent of the gas. On the assumption that the gas in the beam has an extent of one beamwidth, typical gas densities of $n_{\text{H}_2} = 10^4 - 10^5 \text{ cm}^{-3}$ are found.

4. Discussion

These JCMT observations have demonstrated that the OH(1720 MHz) masers in W 44E, W 44F, W 28F and 3C 391 are located near local peaks in the integrated CO $J = 3 - 2$ emission. This hot, dense molecular gas is organized into thin filaments or clumps, with the long axis perpendicular to the shock normal (as inferred from the radio continuum), suggesting compression of the gas by a passing shock. We deduce the existence of the shock from the large observed velocity extent ($\Delta V = 30\text{--}50 \text{ km s}^{-1}$) and the high measured temperature of 80 K. These observations lend

important support to the hypothesis that the OH(1720 MHz) masers originate in the molecular gas behind the shock. We will now attempt to infer the physical properties of the post-shock gas, determine the character of the shock, and investigate models for the shock production and excitation of OH.

In a radiative shock the shock velocity V_s is small enough or the ambient gas density ρ_o is large enough that the timescale for the gas to radiate away its thermal energy, acquired by the passage of the shock, is short compared to the dynamical time of the shock itself (Draine & McKee 1993). The amount of compression expected in this post-shock gas depends in large measure on the strength of the initial magnetic field B_o . The magnetic pressure dominates over the thermal pressure and therefore $\rho_{ps}/\rho_o = \sqrt{2} V_s/V_A$, where V_A is the Alfvén velocity in the ambient gas. It has been customary to estimate B_o using an empirical relation between B and number density n (e.g. Fiebig & Güsten 1989), which shows that over at least 8 orders of magnitude in density $B(\mu\text{G}) = \sqrt{n(\text{cm}^{-3})}$ and implies that $V_A \simeq 1.84 \text{ km s}^{-1}$. Such a relation is not unexpected if there is rough equilibrium between the kinetic and magnetic energy densities in molecular clouds (Myers & Goodman 1988). However, the large observed scatter makes it unreliable to use in individual cases.

The OH(1720 MHz) maser line allows a unique measurement to be made of the strength of the line-of-sight magnetic field B_{los} in the post-shock gas using the Zeeman effect (Claussen et al. 1997). In W 44 and W 28 Claussen et al. (1997) derived an average $B_{los} = 200 \mu\text{G}$ which was remarkably constant in both direction and strength across each remnant. The large scale distribution of magnetic field vectors toward W 44 (Kundu & Velusamy 1972) as traced by the radio synchrotron emission is also uniform. This suggests that these B_{los} values are not some peculiar local values, valid only in the vicinity of the masers, but rather they represent some global measurement in the post-shock magnetic field. For a randomly oriented field, the median value of the total magnetic field strength is $2 \times B_{los}$ and therefore in W 44 and W 28 the post-shock magnetic field $B_{ps} = 400 \mu\text{G}$, and the magnetic pressure $B_{ps}^2/8\pi = 6.4 \times 10^{-9} \text{ erg cm}^{-3}$, or alternatively (see below) $2.7 \times 10^5 \text{ cm}^{-3} (\text{km s}^{-1})^2$.

The magnetic pressure dominates over all other sources of pressure in the post-shock gas, balancing the ram pressure of the gas entering the shock wave $\rho_o V_s^2$. Thus a measurement of B_{los} fixes a line in the n_o - V_s plane which constrains the properties of the post-shock gas from which the OH(1720 MHz) masers originate. In practice there is sufficient uncertainty in B_{ps} that we will consider shocks with a range of ram pressures over 10^5 to $10^6 \text{ cm}^{-3} (\text{km s}^{-1})^2$. Broadly speaking there are two classes of solutions allowed, a dissociative J-shock and a non-dissociative C-shock (Draine & McKee 1993). In a J-shock (for $V_s > 25\text{-}45 \text{ km s}^{-1}$) the physical conditions change abruptly across the shock and molecules can be destroyed. In a C-shock the ions, drifting ahead of the neutrals, produce a more gradual transition and a thicker heating region with limited dissociation of molecules.

If we make the standard assumption that the observed CO $J = 3 - 2$ line widths ΔV of

30-50 km s⁻¹ are giving the shock velocity V_s , then from our ram pressure constraint we infer $n_o \simeq 10^2 - 10^3$ cm⁻³. The final compression in the post-shock gas will depend on V_A in the ambient gas but for the value given above $n_{ps} \simeq 10^4$ cm⁻³. At these relatively low densities the shock is likely to be a dissociative J-type (Draine et al. 1983). A significant column of OH can be formed in the post-shock gas in such a shock (Neufeld & Dalgarno 1989) but the final column density of H₂ never gets sufficiently high to prevent the eventual destruction of the OH by UV photons from the leading edge of the shock. This might explain why the OH masers appear to be confined along the leading edge of the integrated CO maps (see §3). There may be a small region behind the shock where the density and temperature of the OH is sufficient to produce OH(1720 MHz) maser emission, while further downstream the OH is photodissociated.

Another alternative that satisfies our ram pressure constraint would be a slow, non-dissociative C-type shock propagating into denser gas. The true V_s could be smaller than the observed linewidths if the 13'' beam intersected several shocks along the line-of-sight. Furthermore, the detection of H₂CO at the peaks of the integrated CO maps requires the presence of high density post-shock gas $n_{ps} \simeq 10^5 - 10^6$ cm⁻³. Theoretical models (Draine, Roberge & Dalgarno 1983, Kaufman & Neufeld 1996) show that significant columns of warm ($T_k > 1000$ K) OH are produced for $V_s > 15$ km s⁻¹ at a few $\times 10^{16}$ cm behind the leading edge of the disturbance. However, as the gas cools to $T_k \sim 400$ K the models predict that virtually all of the atomic oxygen not tied up in CO will be rapidly converted to H₂O. Wardle, Yusef-Zadeh & Geballe (1998) suggested a novel solution to this problem, dissociating the H₂O by the soft X-rays emitted by the hot gas interior to the remnant. The X-rays penetrate into the dense water-rich gas producing OH in a small region ($\sim 10^{15}$ cm) over which $T_k \sim 100$ -200 K. We consider the Wardle et al. (1998) model to be a particularly promising one since it would explain the apparent narrow region over which we find the OH masers (with respect to the molecular gas) and our measured T_k value.

We thank Bill Reach and Jeonghee Rho for communicating their IRAM results prior to publication and we thank Lorne Avery and Gerald Moriarty-Schieven for their help in setting up the JCMT observing. GFM is supported by the Natural Sciences and Engineering Research Council of Canada. DAF is supported by the NRAO. The NRAO is a facility of the National Science Foundation operated under cooperative agreement by Associated Universities, Inc. The James Clerk Maxwell Telescope is operated by The Joint Astronomy Centre on behalf of the Particle Physics and Astronomy Research Council of the United Kingdom, the Netherlands Organization for Scientific Research, and the National Research Council of Canada.

TABLE 1 – TELESCOPE POINTING PARAMETERS FOR CO $J = 3 - 2$ MAPPING

Name	RA(B1950) (h m s)	Dec(B1950) ($^{\circ}$ ' ")	V_{LSR} km s^{-1}	Ref. (",")	Raster ($" \times "$)
W 28F	17 58 49.2	-23 19 00.0	12	0,-1200	75 \times 110
3C 391	18 46 47.7	-01 01 00.0	105	-120,120	80 \times 80
W 44E	18 53 57.0	+01 25 45.0	45	-760,-1440	75 \times 120
W 44F	18 54 04.7	+01 22 35.0	45	-760,-1440	70 \times 105

Note. — (1) The facility SIS receiver (B3) was used at a center frequency of 345.796 GHz and the signal was fed into a digital autocorrelation spectrometer for a bandwidth of 500 MHz and channel spacing of 378 kHz (0.3 km s^{-1}). (2) The raster maps were made by driving the telescope in right ascension and integrating for 3 seconds at each position separated by $5''$. (3) Sky subtraction was effected by observing a reference position after each row. (4) The beamsize at this frequency is $13''$ and the main beam efficiency is 0.62.

Plate 1.– (left) A $75'' \times 110''$ map of $^{12}\text{CO } J = 3 - 2$ towards a region of OH(1720 MHz) masers known as W 28F. The masers locations are indicated by the filled red circles. The spectra are integrated over the bulk of the emission from -20 km s^{-1} to $+40 \text{ km s}^{-1}$. The color wedge on the right hand side of the plot is the velocity-integrated antenna temperature in units of K km s^{-1} . The shock front, determined from the centimeter radio continuum, lies toward the east. (right) Similar to W 28F but of a $75'' \times 120''$ region toward W 44E. The spectra are integrated from $+20 \text{ km s}^{-1}$ to $+38 \text{ km s}^{-1}$. The shock front lies toward the north east. At the assumed distance of 3 kpc for both W 28 and W 44 the $13''$ beam has a spatial resolution of 0.2 pc.

Copies of this plate can be found at http://www.nrao.edu/~dfraile/jcmt_plate1.gif

Plate 2.– (top) Similar to Plate 1 but of a $80'' \times 80''$ region toward 3C 391. The spectra are integrated from $+60 \text{ km s}^{-1}$ to $+150 \text{ km s}^{-1}$. The shock front lies toward the south west. At the assumed distance of 7.2 kpc for 3C 391 the $13''$ beam has a spatial resolution of 0.45 pc. (Bottom) Similar to 3C 391 but of a $75'' \times 105''$ region toward W 44F. The spectra are integrated from $+49 \text{ km s}^{-1}$ to $+60 \text{ km s}^{-1}$. The shock front lies toward the north east.

Copies of this plate can be found at http://www.nrao.edu/~dfraile/jcmt_plate2.gif

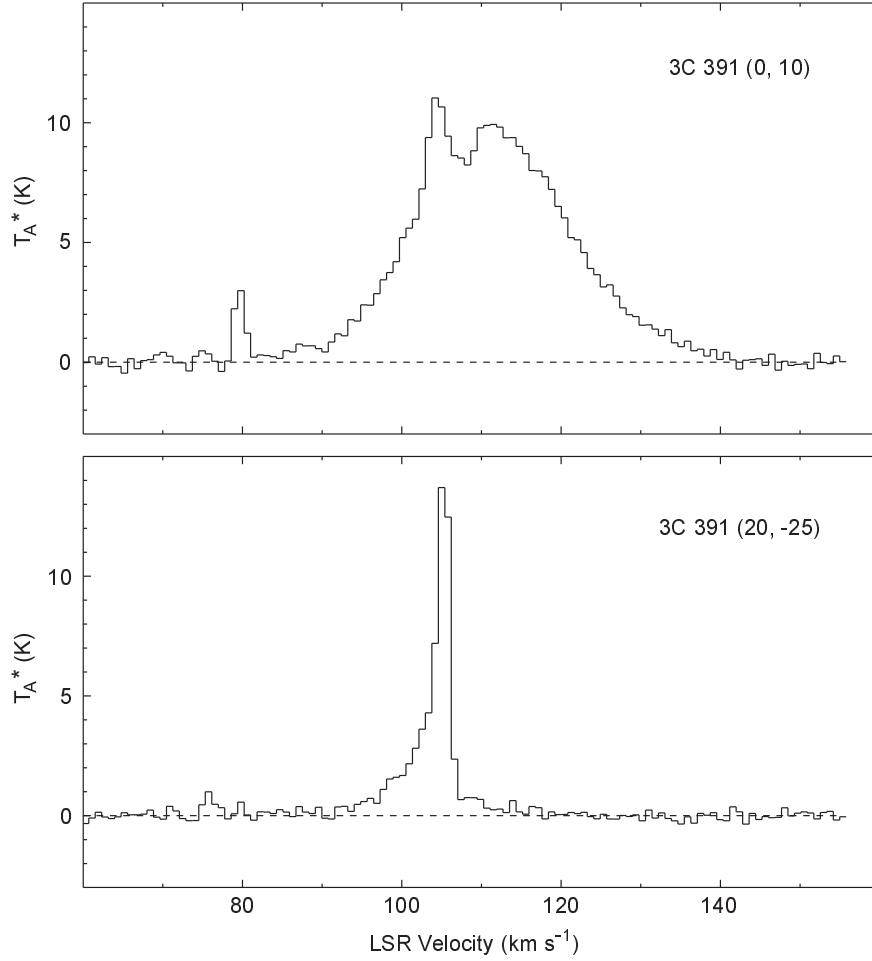


Figure 1.– Sample spectra taken from the $^{12}\text{CO } J = 3 - 2$ map of 3C 391 (Plate 2) at the peaks of the narrow line and broad line emission areas (see main text). These peaks are offset from the map center by $(20'', -25'')$ and $(0'', 10'')$, respectively. The OH(1720 MHz) masers velocity is $+104.9 \text{ km s}^{-1}$. The line brightness on the vertical axis is expressed as antenna temperature T_A^* .

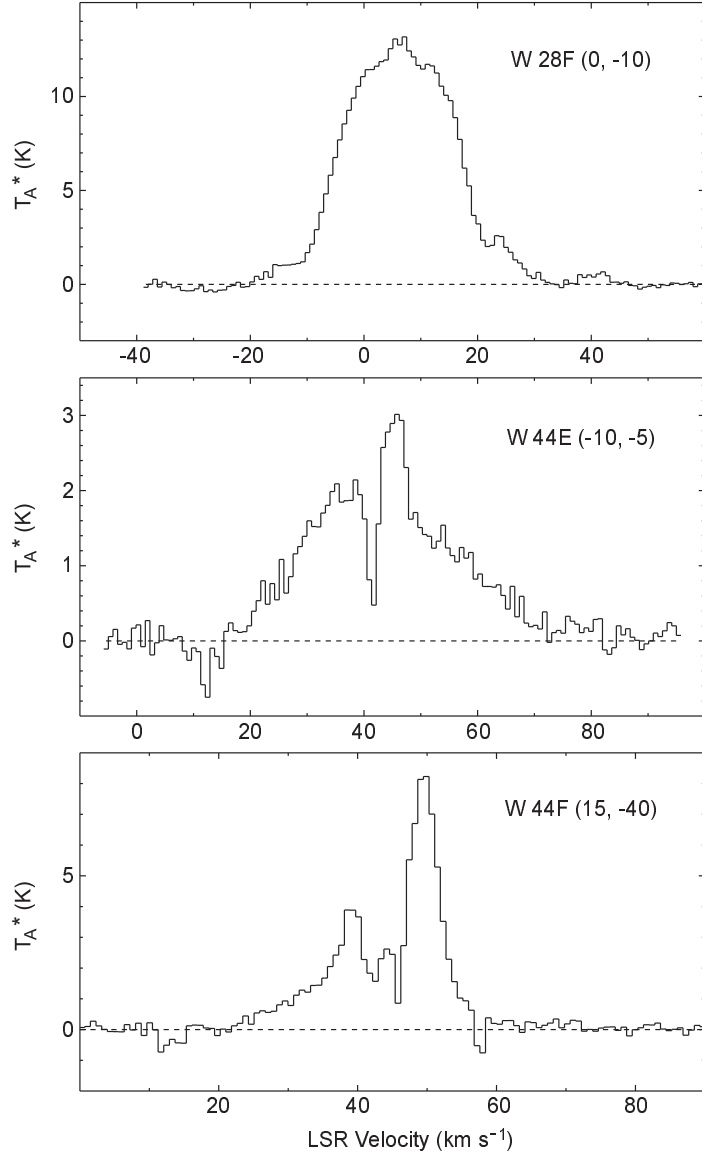


Figure 2.– Sample spectra from the integrated $^{12}\text{CO } J = 3 - 2$ maps of W 28F, W 44E and W 44F. The spectra are taken towards the peaks at position offsets from the center of each map of $(0'', -10'')$, $(-10'', -5'')$ and $(15'', -40'')$, respectively. The pseudo absorption features are likely artifacts produced by emission in the reference position. The average OH(1720 MHz) maser velocities for W 28F, W 44E and W 44F are $+11.0 \text{ km s}^{-1}$, $+44.7 \text{ km s}^{-1}$, and $+46.6 \text{ km s}^{-1}$, respectively.

REFERENCES

- Blandford, R. D., & Cowie, L. L. 1982, ApJ, 260, 625
- Claussen, M. J., Frail, D. A., Goss, W. M., & Gaume, R. A. 1997, ApJ, 489, 143
- Draine, B. T., Roberge, W. G., & Dalgarno, A. 1983, ApJ, 264, 485
- Draine, B. T., & McKee, C. F. 1993, ARA&A, 31, 373
- Elitzur, M. 1976, ApJ, 203, 124
- Elitzur, M., Hollenbach, D. & McKee, C. F. 1989, ApJ, 346, 983
- Fiebig, D., & Güsten, R. 1989, A&A, 214, 333
- Frail, D. A., Goss, W. M., & Slysh, V. I. 1994, ApJ, 424, L111
- Frail, D. A., Goss, W. M., Reynoso, E. M., Giacani, E. B., & Green, A. J. 1996, AJ, 111, 1651
- Green, A. J., Frail, D. A., Goss, W. M., & Otrupcek, R. 1997, AJ, 114, 2058
- Kaufman, M. J., & Neufeld, D. A. 1996, ApJ, 456, 611
- Kundu, M. R., & Velusamy, T. 1972, A&A, 20, 237
- Mangum, J. G. & Wootten, A. 1993, ApJS, 89, 123
- Mitchell, G. F., Hasegawa, T. I., & Schella, J. 1992, ApJ, 386, 604
- Myers, P. C., & Goodman, A. A. 1988, ApJ, 326, L27
- Neufeld, D. A., & Dalgarno, A. 1989, ApJ, 340, 869
- Pavlakis, K. G., & Kylafis, N. D. 1996a, ApJ, 467, 300
- Pavlakis, K. G., & Kylafis, N. D. 1996b, ApJ, 467, 309
- Reach, W. T., & Rho, J. -H. 1996, A&A, 315, L277
- Reach, W. T., & Rho, J. -H. 1998, in preparation
- Straka, W. C., Dickel, J. R., Blair, W. P., & Fesen, R. A. 1986, ApJ, 306, 266
- van Dishoeck, E. F., Jansen, D. J., & Phillips, T. G. 1993, A&A, 279, 541
- Wardle, M., Yusef-Zadeh, F., & Geballe, T. R. 1998, MNRAS, submitted
- Wilner, D. J., Reynolds, & S. P., Moffett, D. A. 1998, AJ, 115, 247

This figure "jcmt_plate1.gif" is available in "gif" format from:

<http://arxiv.org/ps/astro-ph/9807011v1>

This figure "jcmt_plate2.gif" is available in "gif" format from:

<http://arxiv.org/ps/astro-ph/9807011v1>